Computation of Transonic Flows past Lifting Airfoils and Slender Bodies

J. A. KRUPP* AND E. M. MURMAN †
Boeing Scientific Research Laboratories, Seattle, Wash.

Solutions of the transonic small disturbance equation are presented for flow past thin lifting airfoils and slender bodies with $M_\infty < 1$, including cases with imbedded shock waves. The results are obtained numerically using a mixed finite-difference relaxation method previously reported by the authors. Results are presented for four lifting airfoils at various angles of attack and are compared with shock free theory and experimental data. For the slender body case, comparisons with experiments are given for five geometries both with and without aft stings. The results are also compared with approximate theory. Discussion is given on the treatment of the boundary conditions, computing times and accuracies, and ranges of applicability of the small disturbance theory.

Introduction

FOR many cases of engineering interest, the flow about bodies in the transonic regime may be adequately described by transonic small disturbance theory. The basic assumptions of the theory are that the flow is inviscid, the freestream Mach number is close to unity, and that the slope of the body is everywhere small. In practice, the error incurred by these assumptions is not severe except at stagnation points, at large angles of attack, or if extensive flow separation is present. Small disturbance theory contains considerable simplifications over the exact inviscid theory in both the boundary conditions and governing equations. None the less, the resulting transonic potential equation is nonlinear, of mixed elliptic-hyperbolic type, and the solution contains discontinuities (shocks).

Within the context of transonic small disturbance theory the flow about bodies may be divided into three basic regimes, depending on the value of the reduced aspect ratio $\delta^{1/3}AR$ (δ = thickness ratio). For $\delta^{1/3}AR \gg 1$ the flow is essentially two-dimensional and airfoil theory may be used to design wings, rotors, etc. For $\delta^{1/3}AR \ll 1$ the flow is essentially axisymmetric and the transonic equivalence principle holds. For $\delta^{1/3}AR = 0(1)$ the flow is truly three-dimensional. In this paper we treat the first two cases when $M_\infty < 1$. More details and results for the lifting airfoil studies are contained in Ref. 1.

The numerical method used to solve the transonic potential equation has been developed and reported elsewhere by the authors.[2-4] Depending upon whether the local flow is subsonic or supersonic, either an elliptic type or hyperbolic type finite-difference scheme is used to represent the derivatives. An analytic expression derived for the far field is used as an outer boundary condition. The difference equations are solved by a line relaxation algorithm with the elliptic points being overrelaxed. The supersonic region and shock waves appear naturally in the course of the iterations. Convergence is quite good and computing times range from 3 to 20 min on an IBM 360/65 for typical mesh spacings used and accuracy desired. Exceptional cases can require more or less computer time. The converged solution contains essentially complete information about both the body surface properties (pressure, etc.) and flowfield properties.

Presented as Paper 71-566 at the AIAA 4th Fluid and Plasma Dynamics Conference, Palo Alto, Calif., June 21–23, 1971; submitted June 10, 1971; revision received March 2, 1971.

Index categories: Subsonic and Transonic Flow; Airplane and Component Aerodynamics.

* Staff Member; presently at the University of California at Los Angeles, Department of Mathematics.

† Staff Member; presently at NASA Ames Research Center, Moffett Field, Calif. Member AIAA.

Lifting Airfoil Results

Consider an airfoil with upper and lower surfaces given by $y_{u,l} = \delta f_{u,l}(x)$, $|x| \leqq 1$, where x and y are nondimensional coordinates and $\max|f_{u,l}(x)| = 1$. For the case of thin airfoils, $\delta \ll 1$, at small angle of attack, $\alpha \ll 1$, in a nearly sonic freestream, a singular perturbation analysis applied to the equations of steady, two-dimensional isentropic flow yields the following equation and boundary conditions for the perturbation potential ϕ

$$\begin{gathered}(K-(\gamma+1)\phi_x)\phi_{xx}+\phi_{\tilde{y}\tilde{y}}=0\\ \phi_{\tilde{y}}(x,0\pm)=f'_{u,l}(x)-A;\quad |x|\leqq 1\\ \phi_x,\phi_{\tilde{y}}\to 0\quad\text{as}\quad x^2+\tilde{y}^2\to\infty\end{gathered}\tag{1}$$

In this equation γ, the ratio of specific heats, is constant, and $\tilde{y} = (M_\infty{}^2\delta)^{1/3}y$. A and K are similarity parameters for the problem. The choice of A is fixed by the boundary conditions as $A = \alpha/\delta$. There exists some degree of arbitrariness in the choice of K. This is also true of the pressure coefficient C_p which is proportional to the perturbation velocity ϕ_x. A choice for these two quantities which best correlates numerical solutions to Eq. (1) with certain exact solutions to the full inviscid equations is given by[1]

$$K = (1-M_\infty{}^2)/M_\infty\delta^{2/3};\quad C_p = -2(\delta^{2/3}/M_\infty{}^{3/4})\phi_x \tag{2}$$

In addition to the boundary conditions in Eq. (1), a solution for an airfoil with a sharp trailing edge must satisfy the Kutta condition. Within the framework of small disturbance theory, this reduces to a requirement that ϕ_x and $\phi_{\tilde{y}}$ be continuous across the line $\tilde{y} = 0$, $x > 1$. The circulation γ_0 is defined by

$$\gamma_0 = -\oint d\phi$$

for any path enclosing the slit $y = 0$, $|x| < 1$. For $\gamma_0 \neq 0$, ϕ will be multiple valued unless a cut is introduced into the $(x, \tilde{y})$ plane across which ϕ jumps in value by an amount γ_0. This cut is chosen to be the line $\tilde{y} = 0$, $x > 1$. The required continuity of ϕ_x and $\phi_{\tilde{y}}$ across this line can be obtained by the proper choice of γ_0.

Numerical procedures for external problems like Eqs. (1) are often handled by transforming the problem into another plane. This allows for both the treatment of the infinity boundary condition and the Kutta condition in a direct manner.[5] An alternate approach is to solve the problem in the plane in which it is posed, and to treat the infinity boundary condition in an approximate manner.[2] We adopt the latter approach. Details of

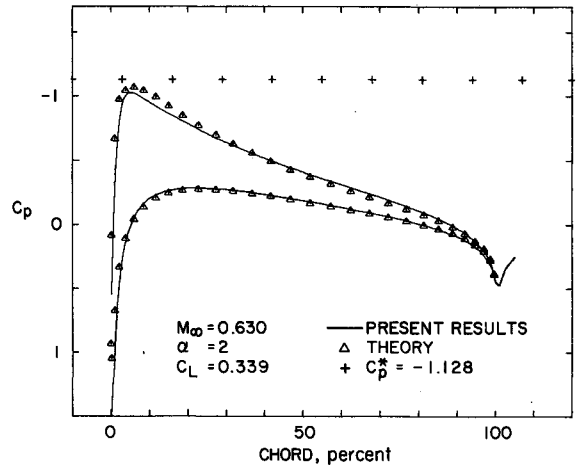

Fig. 1 Comparison with Sells' solution for a NACA 0012 airfoil.

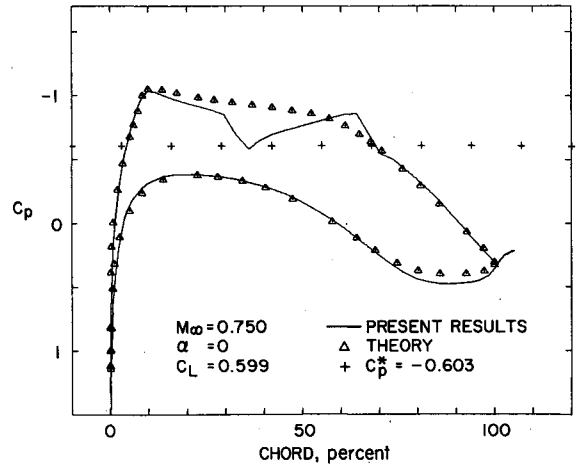

Fig. 3 Comparison with exact solution Garabedian and Korn airfoil at design (shock-free) conditions.

the derivation of the far field solution are given in Ref. 1. The basic result is

$$\phi(x,\tilde{y}) = \frac{1}{\pi K^{1/2}}\mathscr{R}e\int_{-1}^{1} t'(\xi)\log(z-\xi) - [c'(\xi)-A]\times \log\left\{\frac{\xi z - 1 + [(z^2-1)(\xi^2-1)]^{1/2}}{z-\xi}\right\} d\xi - \frac{\gamma_0}{2\pi}\arg[z+(z^2-1)^{1/2}] \quad (3)$$

where $z = x + iK^{1/2}\tilde{y}$. The expression $(z^2-1)^{1/2}$ is positive for z real and greater than one, where the branch cut is along $y = 0$, $|x| < 1$, and $0 < \arg < 2\pi$. This approximate result is sufficiently accurate if the boundary of the region is far enough from the origin ($|\tilde{y}_{max}| \simeq 6$; $|x_{max}| \simeq 3$). In Eq. (3) γ_0 is the circulation defined above and its value depends upon ϕ and must be determined as part of the solution for ϕ. This differs from a linear problem where circulation is determined entirely from the boundary conditions on the slit $\tilde{y} = 0$, $|x| < 1$, and the continuity of ϕ_x.

A convergent procedure for determining γ_0 as part of the solution for ϕ was found that does not require monitoring of intermediate results. Difference formulas for $\phi_{\tilde{y}\tilde{y}}$ along the line $\tilde{y} = 0$, $x > 1$, take into account the jump in ϕ across this line and implicitly assume the continuity of ϕ_x and $\phi_{\tilde{y}}$. For example let $x_i = i\Delta x$, $\tilde{y}_j = j\Delta\tilde{y}$, and $\phi_{i,j} = \phi(x_i, \tilde{y}_j)$, where $i = 0, \pm 1, \pm 2, \ldots, \pm i_{max}$, $j = 0, \pm 1, \pm 2, \ldots, \pm j_{max}$. Let $\tilde{y}_0 = 0-$ and $\phi(x_i, 0+) - \phi(x_i, 0-) = \sigma_i$ for $x_i > 1$. In the converged solution $\sigma_i = \gamma_0$. Then the difference approximation to Eq. (1) at $(x_i, \tilde{y}_0)$ will have $\phi_{\tilde{y}\tilde{y}}$ differenced in the modified form

$$\phi_{\tilde{y}\tilde{y}}|_{i,0} = \frac{1}{\Delta\tilde{y}}\left[\frac{(\phi_{i,1}-\sigma_i)-\phi_{i,0}}{\Delta\tilde{y}} - \frac{\phi_{i,0}-\phi_{i,-1}}{\Delta\tilde{y}}\right] \quad (4)$$

A similar result for points $(x_i, \tilde{y}_1)$ holds. With this modification the same line relaxation technique as in Refs. 2–4 is used. Let some initial value of γ_0 be given and define $\gamma_{te} = \phi(1,0+) - \phi(1,0-)$. On each sweep through the region a new value of γ_{te} is found which, with the present value of γ_0, is used to determine σ_i by linearly interpolating between γ_{te} and γ_0. This procedure is repeated a prescribed number of times, or until $(\gamma_{te} - \gamma_0)$ changes sign. At this point a new value of γ_0 is found by extrapolating from past values of γ_0 and γ_{te}. This entire process is now repeated until a converged solution for ϕ is obtained.

The numerical solution to Eq. (1) is inaccurate near $(-1, 0)$. However, the error is dominated by the error of small disturbance theory near the nose. The cause is the singularity associated with the existence of a stagnation point so that disturbances are not small. In addition, for an airfoil at angle of attack the leading edge stagnation point moves away from the true leading edge, resulting in a rapid expansion around the nose. The linearized boundary condition always places this stagnation point at the nose, and hence for any appreciable angle of attack, loses this expansion. For most airfoils this is not critical, but for certain designs there is enough error to cause deviation between small disturbance theory and exact theory or experiment. Numerical experimentation showed that a refined mesh adequately handled this singularity.

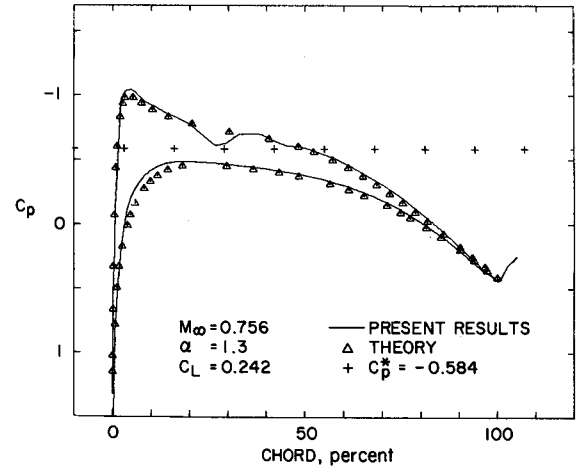

Fig. 2 Comparison with exact solution for NLR quasi-elliptical airfoil at design (shock-free) conditions.

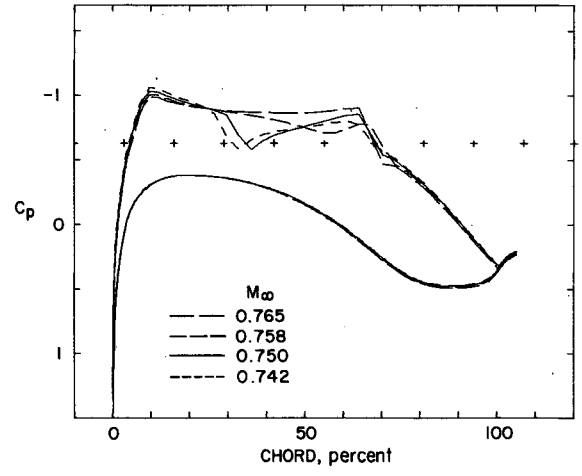

Fig. 4 Variation of C_p distribution with M_∞ for Garabedian-Korn airfoil near design conditions.

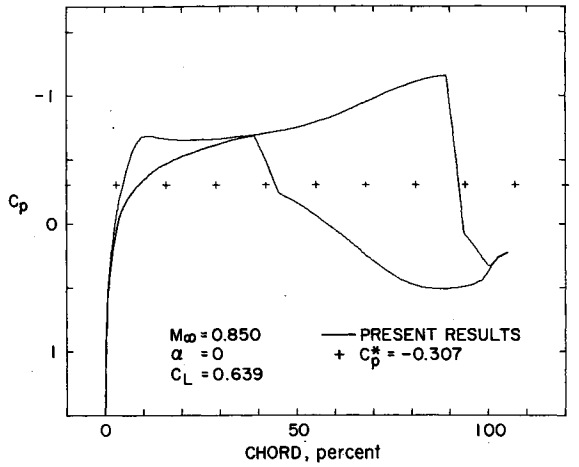

Fig. 5 Off design condition for Garabedian-Korn airfoil.

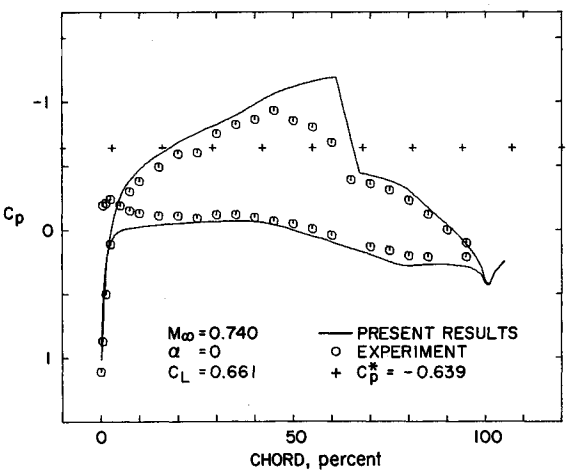

Fig. 7 Comparison with experimental data of Stivers for 64A410 airfoil.

Figures 1–9 present results obtained using the above procedure on four different airfoils. Figure 1 compares results of the present method with a numerical solution to the full inviscid equations for subcritical flow past an NACA 0012 airfoil at 2° angle of attack. The agreement is excellent, particularly considering the low Mach number (0.63) for transonic small disturbance theory. Figure 2 is a shockless NLR quasi-elliptical airfoil at angle of attack of 1.3°. Flows past shock free airfoils have been found to be very sensitive to small changes in Mach number and body shape. As such, the weak shock wave in the numerical solution is not at all surprising considering the small disturbance theory approximations. Both of these examples were chosen as standard test problems for transonic flow calculations as is suggested by Lock.[6] Figures 3–6 are solutions to another shock free airfoil.[7] Figure 3 compares the present results with the exact theory for the design Mach number. Figure 4 shows the sensitivity of this design to small variations in freestream Mach number. These results concur with the findings of Kacprzynski et al.[8] Figures 5 and 6 show this airfoil at off-design conditions. There was no data available for comparison at the time of this writing. The condition of Fig. 6 was chosen in an attempt to get a zero lift condition. The angle of attack $-2.8°$ is in agreement with predictions of the airfoil's designer. Figures 7 and 8 show results for an NACA 64A410 airfoil compared with the results obtained experimentally by Stivers.[9] The experimental data was obtained at $Re_l \cong 2 \times 10^6$ in a low-turbulence wind tunnel with solid walls. The resulting viscous effects and wall interference account for most of the deviation present between computed results and the data. The deviation of C_p on the lower surface near the nose is possibly due to the moving of the stagnation point, resulting in a greater expansion near the nose than the numerical solution would compute. Figure 8 is a comparison with the case computed by Magnus and Yoshihara[10] using a time dependent method. The four degree angle of attack is large for the small disturbance approximation, but over-all the agreement is still reasonable. The deviation between the two computed solutions is probably the result of different circulation in the solutions. This is difficult to ascertain since the authors of Ref. 10 do not discuss this point. Figure 9 shows a result for the NACA 0012 airfoil. Agreement with existing data is about the same as for the 64A410 airfoil and has been omitted here since it serves no strong indication as to the accuracy of the computed results.

These results were obtained using single precision arithmetic on an IBM 360/44. The grid used has 75 points in the x direction with 48 points between -1 and $+1$; there are 60 points in the y direction (30 on each side of $\tilde{y} = 0$). Computational times vary from 15 min to over an hour for runs of 250 to 1200 iterations (this is equivalent to 5–20 min on an IBM 360/65). Convergence is established by requiring the circulation to stabilize to within 0.1% for 20 iterations. The circulation for various paths in the flowfield is also computed and required to agree with this value. A mass flux integral from Eq. (1) is also integrated over various paths and required to be small, about 10^{-2}. These criteria are met when a relative change in ϕ between iterations of less than 10^{-4} occurs. This degree of convergence is not required for most engineering applications, and the lower limits

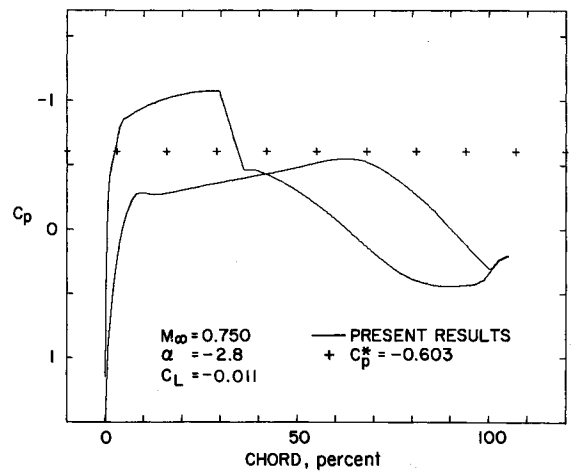

Fig. 6 Garabedian-Korn airfoil near zero lift angle of attack and design M_∞.

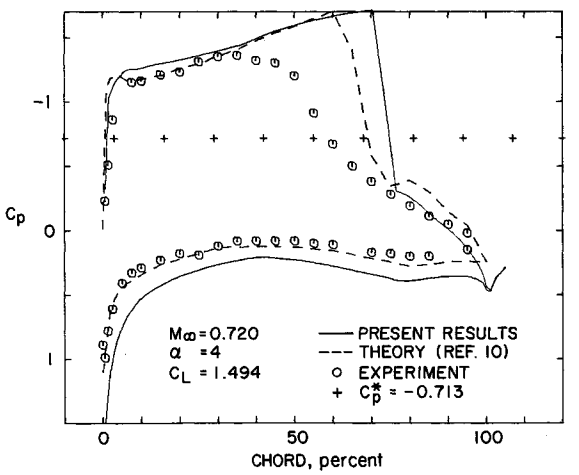

Fig. 8 Comparison with calculations of Magnus and Yoshihara and experimental data of Stivers for 64A410 airfoil.

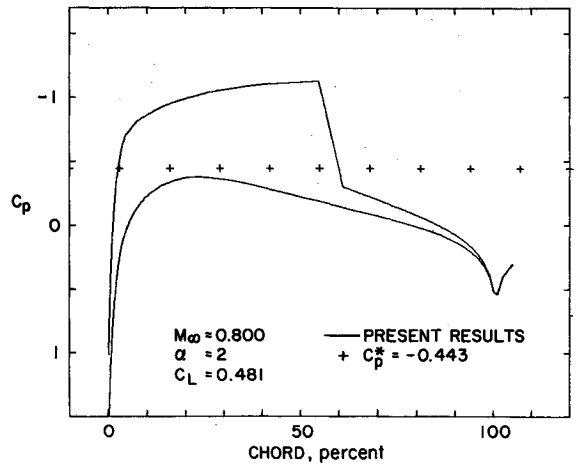

Fig. 9 Solution for NACA 0012 airfoil.

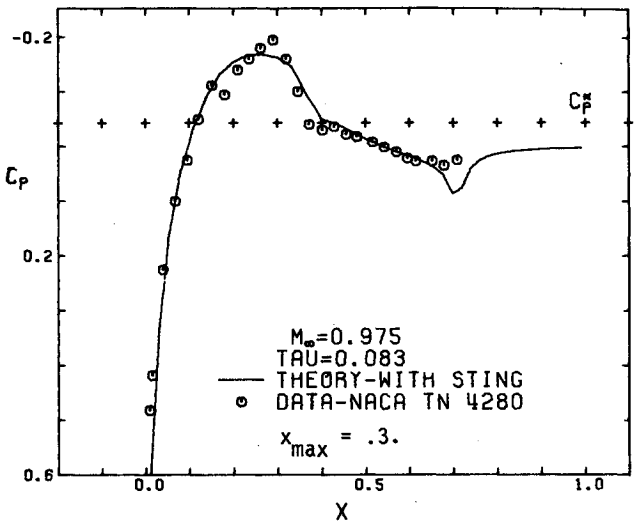

Fig. 10 Comparison with data of McDivitt and Taylor for axisymmetric body with maximum thickness at $X = 0.3$.

on time and number of iterations, particularly for a somewhat coarser mesh, give a solution to within 5 per cent of the fully converged result.

Slender Body Results

The solution for small disturbance transonic flow about a slender body is obtained by solving for the transonic flow about an equivalent axisymmetric body and properly combining this with the solution for the incompressible flow in each cross section plane. For the remainder of this paper we report on a solution procedure for the axisymmetric transonic small disturbance equation

$$[K-(\gamma+1)\phi_x]\phi_{xx}+(1/\tilde{r})(\tilde{r}\phi_{\tilde{r}})_{\tilde{r}}=0 \tag{5}$$

This equation is identical to Eq. (1) except for the usual axisymmetric effects in the $\tilde{r}$ derivatives and the different definition for K and $\tilde{r}$ given by

$$K=(1-M_\infty{}^2)/(M_\infty\tau)^2; \quad \tilde{r}=\tau r \tag{6}$$

The parameter τ is the thickness ratio of the body (inverse fineness ratio) defined by the formula for the body shape $r_b(x)=\tau R(x)$. We choose the body length to be 1 and the maximum nondimensional radius $R_{\max}(x)=0.5$.

The body boundary condition for Eq. (5) must be derived by matching to an inner solution due to the singular nature of the flow as $\tilde{r}\to 0$. The result is that

$$\lim_{\tilde{r}\to 0}(\tilde{r}\phi_{\tilde{r}})=S'(x) \tag{7}$$

or

$$\lim_{\tilde{r}\to 0}\phi=S'(x)\ln\tilde{r}+g(x) \tag{8}$$

where $S(x)=R(x)^2/2$ is the nondimensional cross section area divided by 2π. Thus, the inner flow is known except for a function $g(x)$, which must be determined by matching to the outer solution governed by Eq. (5).

At large distances from the body the perturbation velocities must vanish. For finite difference computations this condition may be replaced with an asymptotic solution for Eq. (5) derived from the corresponding integral equation evauated at large distances from the body. The result for the present problem is

$$\phi(x,\tilde{r})=\frac{-S_0}{2(\bar{x}^2+K\tilde{r}^2)^{1/2}}+\frac{1}{4}\Bigg[-S_0+2\int_0^{x_0}S(\xi)\,d\xi+(\gamma+1)\int\int_{-\infty}^{\infty}\phi_x{}^2(\xi,\rho)\rho\,d\rho\,d\xi\Bigg]\frac{\bar{x}}{(\bar{x}^2+K\tilde{r}^2)^{3/2}}+\dots \tag{9}$$

We assume the body extends from $x=0$ to $x=1$, and $\bar{x}\equiv x-\frac{1}{2}$. S_0 can either be the base area of the body (generally zero) in which case $x_0=1$, or the area of a sting attached to the basic body shape at some location $x_0<1$. The far field is seen to have the form of an axisymmetric source if $S_0\neq 0$ and an axisymmetric doublet (plus higher order terms) located at the center of the body. The strength of the doublet is made up of a first order correction term to the axisymmetric source, the volume of the body, and a contribution from the nonlinear term which is unknown in advance.

To complete the formulation of the problem we write down the formula for the pressure coefficient in the outer region

$$C_p=-2\tau^2\phi_x$$

and the formula for the pressure on the body

$$C_p(x,\tilde{r}=R)=-\tau^2[2S''\ln(M_\infty\tau^2R)+(R')^2+2g'(x)]$$

The latter formula includes the cross flow contribution which is important near the body.

The x derivatives in Eq. (5) are replaced by the same difference equations as used in the two-dimensional studies.[2-4] A centered difference formula is used for the $\tilde{r}$ derivatives. The equations are written for unequal mesh spacing so that the location of the mesh points is arbitrary. On the outer boundaries of the mesh domain ϕ is specified from Eq. (9). The double integral is evaluated over the mesh domain after every 10 iterations using a trapezoidal

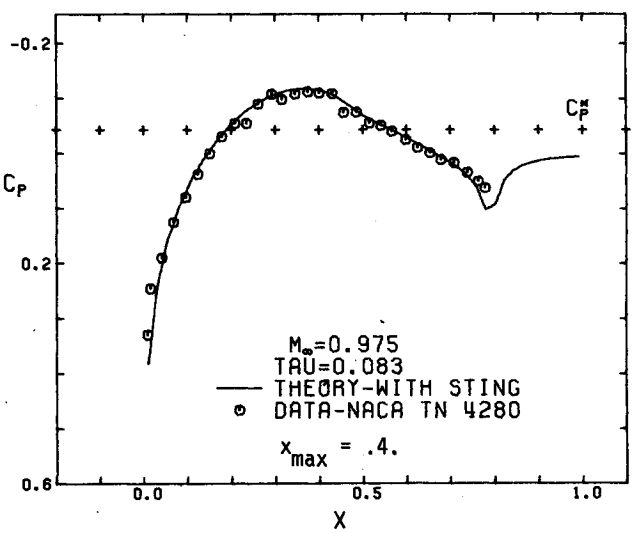

Fig. 11 Comparison with data of McDivitt and Taylor for axisymmetric body with maximum thickness at $X = 0.4$.

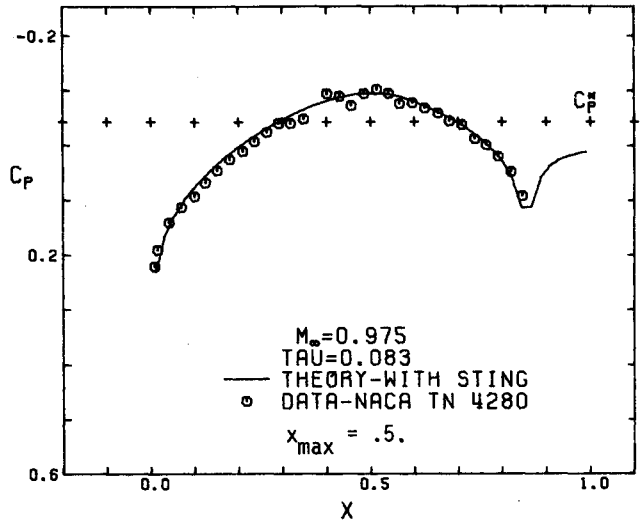

Fig. 12 Comparison with data of McDivitt and Taylor for axisymmetric body with maximum thickness at $X = 0.5$.

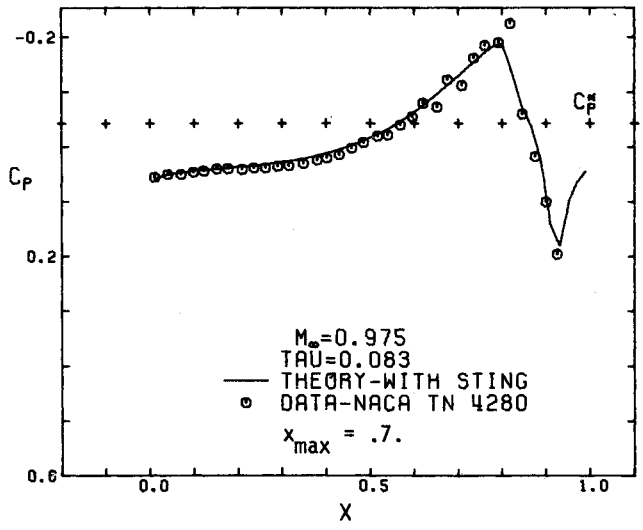

Fig. 14 Comparison with data of McDivitt and Taylor for axisymmetric body with maximum thickness at $X = 0.7$.

integration routine. The contribution to the integral from outside of the mesh domain is neglected. The convergence of the calculations are fairly insensitive to the details of this iteration on the outer boundary condition.

It was found best to apply the body boundary condition Eq. (7) at a small finite radius $\tilde{r}_1$ rather than on the axis due to the logarithmic singularity in ϕ. From numerical experimentation and comparison with an exact solution for the linear equation it was found that a choice of $\tilde{r}_1 K^{1/2} = 0.015$ was best. For values of K less than one, $\tilde{r}_1$ was held fixed at 0.015.

Several spacings and numbers of mesh points were tried. The results reported here were all computed using 82 mesh points in the x direction (38 on the body) and 30 in the $\tilde{r}$ direction. Near the axis the mesh points were spaced exponentially in $\tilde{r}K^{1/2}$ and farther away even mesh spacing was used out to $\tilde{r}K^{1/2} = 3$. For $K < 1$, the factor of $K^{1/2}$ is set equal to one. In the x direction the mesh extended 3 body lengths ahead and behind the body. A nonuniform distribution was used over the body with more mesh points near the nose and aft 40% of the chord. It is an easy matter to change the x-mesh spacing to suit the particular body geometry.

Various values of ω, the overrelaxation parameter for elliptic points, were tried and $\omega = 1.90$ was found to be near optimum. Anywhere from 150 to 500 iterations were required for convergence depending on the value of K and the initial values used for ϕ. Convergence was determined by examining the surface pressures and drag coefficient. In all cases, for a converged solution, the value of C_D was changing by less than 10^{-4} during 5 iterations. The computations required from 8–20 min of IBM 360/44 computer time (approximately 3–7 min of IBM 360/65 time).

Results have been computed for five slender body geometries with fineness ratios from 6 to 12 and Mach numbers from 0.85 to 0.999. This corresponds to a variation in K from about 27.0 to 0.20. Most bodies have been computed both with and without aft stings for comparison with experimental data. The bodies belong to a class of generalized parabolic arcs of revolution which have the location of the maximum thickness ranging from 30% to 70% of the body length in increments of 10%. The equations for the bodies are given in Ref. 11.

Figures 10–14 present results for the five bodies each with a fineness ratio of 12 and at $M_\infty = 0.975$. The data were obtained by McDivitt and Taylor[11] in the NASA Ames 14 foot transonic tunnel which had slotted walls with corrugated strip inserts. The models were 72 in. long and the Reynolds number based on body length was about 24×10^6. No corrections were made for

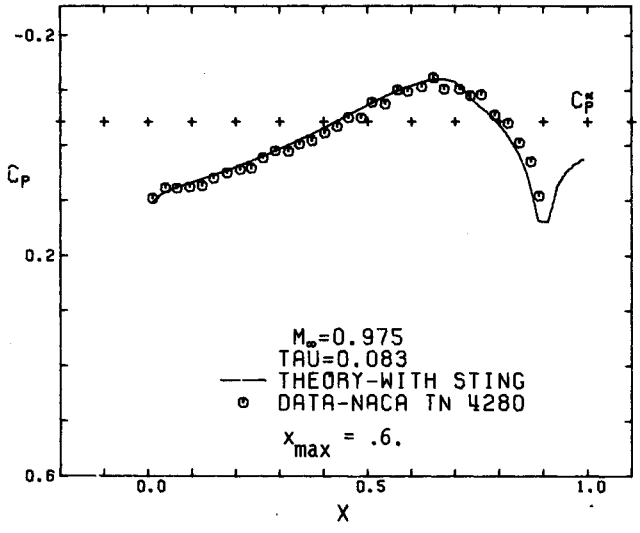

Fig. 13 Comparison with data of McDivitt and Taylor for axisymmetric body with maximum thickness at $X = 0.6$.

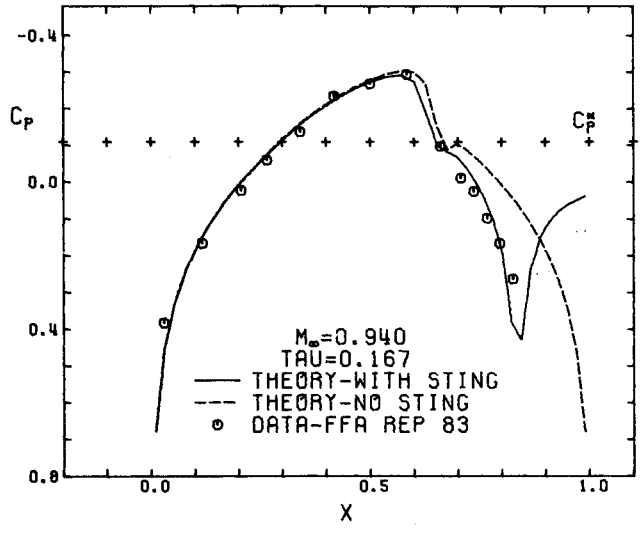

Fig. 15 Comparison with data of Drougge for parabolic arc of revolution at $M_\infty = 0.94$.

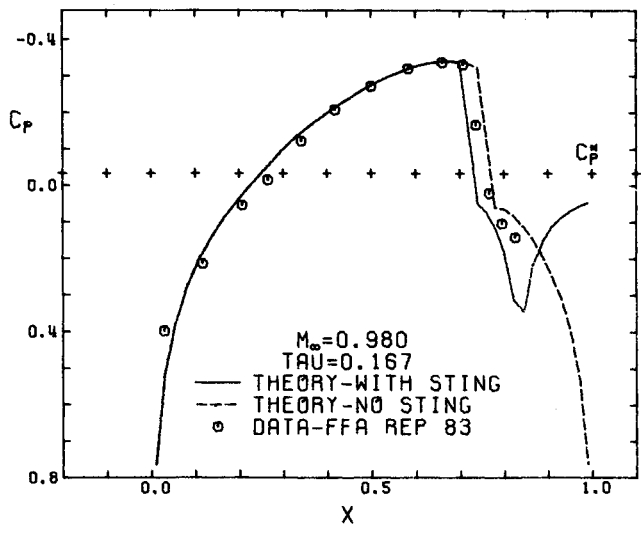

Fig. 16 Comparison with data of Drougge for parabolic arc of revolution at $M_\infty = 0.98$.

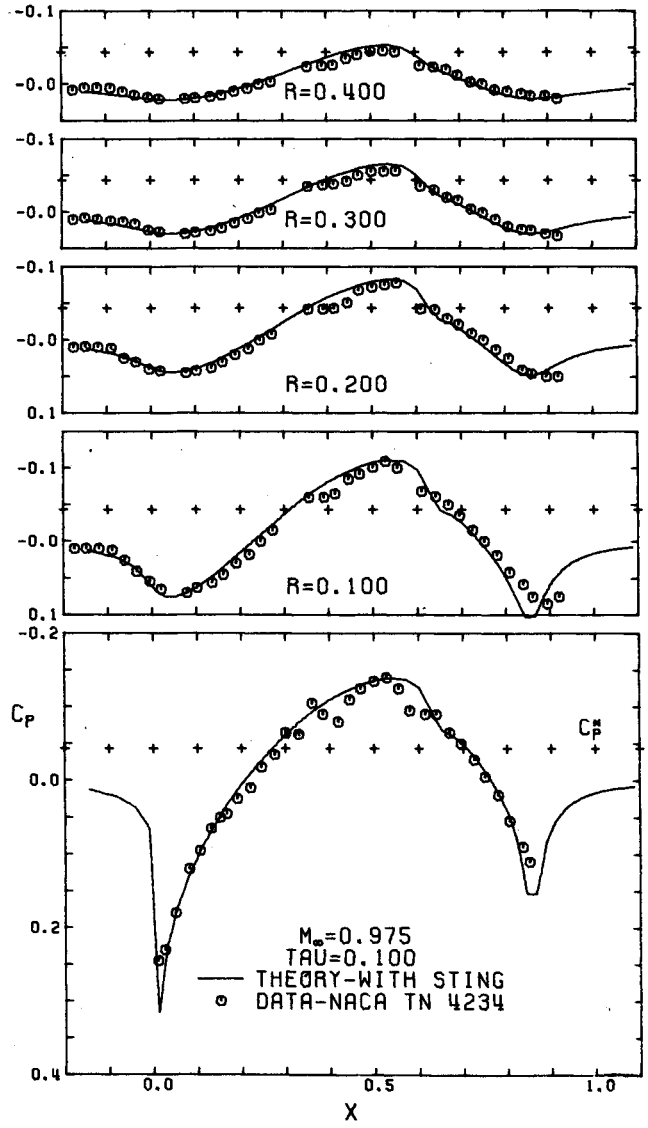

Fig. 17 Comparison with surface and flowfield data of Taylor and McDivitt for parabolic arc of revolution.

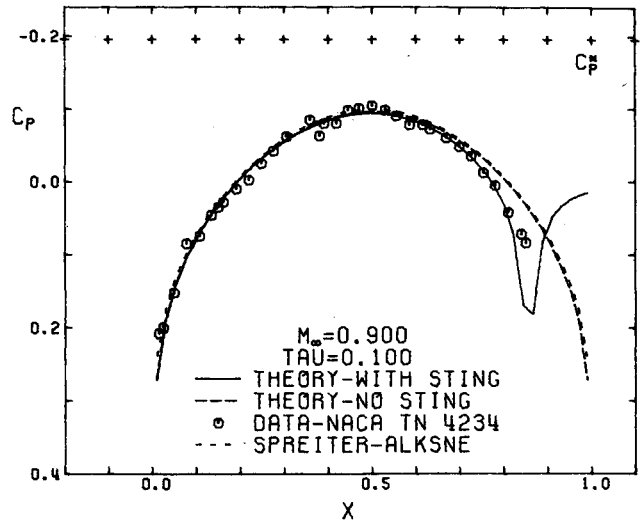

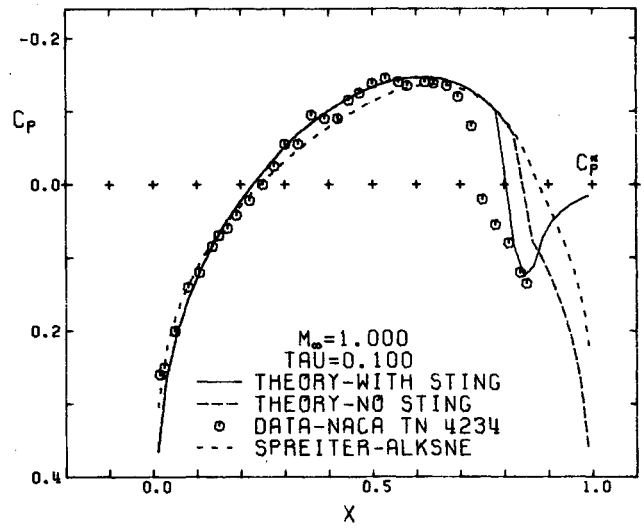

Fig. 18 Comparison with theory of Spreiter and Alksne and data of Taylor and McDivitt for parabolic arc of revolution.

any wall interference effects. Agreement between theory and experiment is very good with minor exceptions. There is some disagreement at the body-sting junction as might be expected from boundary-layer effects. No special treatment was made in the calculation for the discontinuous change in body shape at that location.

In Figs. 15 and 16 computed results for a parabolic arc of revolution of fineness ratio 6 both with and without aft sting are compared with data measured by Drougge.[12] These data were obtained in the FFA 18 × 19 in. slotted wall wind tunnel with a 5.6 in. long model ($Re_l \simeq 2 \times 10^6$). Again, the theory and data are in excellent agreement with minor exceptions. Of particular interest is the effect of the aft sting on the measured pressures which can be clearly ascertained from the computed results. It is also worthwhile noting that small disturbance theory accurately predicts the pressures even for this relatively thick body, $\tau = 0.167$, a fact which has generally been known from scaling experimental data using the small disturbance similarity rules.

Comparisons between calculated and measured pressures on the body and at several radial locations in the flowfield of a fineness ratio 10 parabolic arc of revolution at $M_\infty = 0.975$ are given in Fig. 17. The data were obtained by Taylor and McDivitt[13] using the NASA tunnel mentioned above with an 80″ long model. Good agreement is apparent throughout the flowfield except in the region most affected by the body-sting junction flow, where viscous effects are important. Thus it is evident that the

computational method is useful for predicting the entire flowfield.

Finally, in Fig. 18 comparisons are shown between the present results, results of the local linearization theory of Spreiter and Alksne[14] and experimental data of Taylor and McDivitt[13] for a subcritical case ($M_\infty = 0.90$) and sonic flow ($M_\infty = 1.0$) past a fineness ratio 10 parabolic arc of revolution. The present computations are at $M_\infty = 0.999$ which is within the experimental accuracy ($\Delta M = \pm 0.002$) of sonic flow. For the $M_\infty = 0.9$ case, the present calculations without aft sting and the Spreiter and Alksne results are nearly indistinguishable. The theories without the sting are symmetrical fore and aft of the body midpoint, while the calculation with the sting present agrees with the measured results. For the $M_\infty = 1$ case the present computations are in better agreement with the data than the Spreiter and Alksne theory except over the forward 10% of the body. The present calculations predict a shock wave location farther downstream than the measured location. Wall tunnel interference could well be responsible for this as the wind-tunnel wall is only about 1 body length away from the body. It is also interesting to note that at $M_\infty = 1$ the shock wave is well upstream of the body terminus.

Conclusions

Methods have been developed for numerically solving the transonic small disturbance equation for flow past thin lifting airfoils and slender bodies. Extensive calculations have been performed for a number of bodies. The results have been compared with exact shock free theory, approximate theories and experimental data. From these comparisons we conclude that the computational procedures are useful for many engineering applications. Both blunt nosed airfoils and relatively thick bodies (10–15%) may be treated using transonic small disturbance theory. The principal limitations arise from occurrence of extensive separated flow regions (viscous effects) and inaccuracies in the leading edge region of lifting airfoils with high-nose camber or at moderate to large angle of attack. The computational methods are stable, reliable, and relatively fast.

References

[1] Krupp, J. A., "The Numerical Calculation of Plane Steady Transonic Flows Past Thin Lifting Airfoils," Ph.D. dissertation, June 1971, Univ. of Washington, Seattle, Wash.; also Boeing Scientific Research Labs. document D180-12958-1, June 1971.

[2] Murman, E. M. and Cole, J. D., "Calculation of Plane Steady Transonic Flows," *AIAA Journal*, Vol. 9, No. 1, Jan. 1971, pp. 114–121.

[3] Murman, E. M. and Krupp, J. A., "Solution of the Transonic Potential Equation Using a Mixed Finite Difference System," *Proceedings of the 2nd International Conference on Numerical Methods in Fluid Dynamics, Lecture Notes in Physics*, Springer-Verlag, 1971.

[4] Murman, E. M., "Computational Methods for Inviscid Transonic Flows with Imbedded Shock Waves," document D1-82-1053, Feb. 1971, Boeing Scientific Research Labs.

[5] Sells, C. C. L., "Plane Subcritical Flow Past a Lifting Airfoil," RAE TR 67146, June 1967, Royal Aircraft Establishment, England.

[6] Lock, R. C., "Test Cases for Numerical Methods in Two-Dimensional Transonic Flows," AGARD Rept. 575, Nov. 1970.

[7] Garabedian, P. R. and Korn, D. G., "Numerical Design of Transonic Airfoils," *Numerical Solution of Partial Differential Equations—II*, Academic Press, 1971.

[8] Kacprzynski, I. J., Ohman, L. H., Garabedian, P. R., and Korn, D. G., "Analysis of Flow Past the Shockless Lifting Airfoil, Design and Off-Design Condition," AIAA Paper 71-567, Palo Alto, Calif., 1971.

[9] Stivers, L., "Effects of Subsonic Mach Number on the Forces and Pressure Distribution of Four NACA 64A-Series Airfoil Sections," TN 3162, 1954, NACA.

[10] Magnus, R. and Yoshihara, H., "Inviscid Transonic Flow Over Airfoils," *AIAA Journal*, Vol. 8, No. 12, Dec. 1970, pp. 2157–2162.

[11] McDivitt, J. B. and Taylor, R. A., "Pressure Distributions at Transonic Speeds for Slender Bodies Having Various Axial Locations of Maximum Diameter," TN 4280, 1958, NACA.

[12] Drougge, G., "An Experimental Investigation of the Interference Between Bodies of Revolution at Transonic Speeds, with Special Reference to the Sonic and Supersonic Area Rules," FFA, Rept. 83, 1959, Aeronautical Research Inst. of Sweden.

[13] Taylor, R. A. and McDivitt, J. B., "Pressure Distributions at Transonic Speeds for Parabolic-Arc Bodies of Revolution Having Fineness Ratios of 10, 12, and 14," TN 4234, 1957, NACA.

[14] Spreiter, J. R. and Alksne, A. V., "Slender-Body Theory Based on Approximate Solution of the Transonic Flow Equation," TR R-2, 1958, NASA.